

Backscattering enhancement with a finite beam width for millimeter-wavelength weather radars

Satoru Kobayashi^a, Simone Tanelli^a, Toshio Iguchi^b, and Eastwood Im^a

^aJet Propulsion Laboratory California Institute of Technology, 4800 Oak Grove Dr.
MS.300-243, Pasadena, CA 91109, USA

^bNational Institute of Information and Communications Technology, 4-2-1 Nukui-kita,
Koganei, 184-8795, Japan

ABSTRACT

Backscattering enhancement from random hydrometeors should increase as wavelengths of radars reach millimeter regions. For 95 GHz radars, the reflectivity of backscattering is expected to increase by 2 dB, due to multiple scattering including backscattering enhancement, for water droplets of diameter of 1 mm with a density of $5 \times 10^3 \text{ m}^{-3}$. Previous theoretical studies of backscattering enhancement considered infinitely extending plane waves. In this paper, we expand the theory to spherical waves with a Gaussian antenna pattern, including depolarizing effects. While the differences from the plane wave results are not great when the optical thickness is small, as the latter increases the differences become significant, and essentially depend on the ratio of radar footprint radius to the mean free path of hydrometeors. In this regime, for a radar footprint that is smaller than the mean free path, the backscattering-enhancement reflectivity corresponding to spherical waves is significantly less pronounced than in the case of the plane wave theory. Hence this reduction factor must be taken into account when analyzing radar reflectivity factors for use in remote sensing applications.

Keywords: backscattering enhancement, multiple scattering, weather radar

1. INTRODUCTION

Millimeter-wavelength weather radars have been extensively used to increase accuracy of measuring hydrometeor number densities (e.g. raindrops, liquid-cloud particles). In this frequency regime, multiple scattering effects become important so as to be taken into account when using radar reflective intensity in retrieval algorithms of hydrometeor density. The occurrence of multiple scatterings was confirmed in 35 GHz radar measurements by the presence of depolarized signals reflected from spherical rain drops.^{1,2}

From the early 1970's to the early 1990's, multiple scattering in randomly distributed particles was intensively studied through the analytical method of electromagnetic wave.³⁻⁷ In the course of study, two main contributions of multiple scattering to reflective intensity were revealed as follows: The electromagnetic field reflected from random media can be represented as a sum of fields from many portions of the media. Among this sum, only pairs of fields that have strong correlation can give contributions to a measured intensity. A first possible pair is constituted of a field E_A and its self-complex-conjugate field E_A^* as depicted in Fig. 1a in the case of the second order scattering. In the figure, the field E_A is transmitted from the antenna T, and scatters at point b and a successively, eventually returning to the antenna T. This scheme can be represented by the second order ladder diagram shown in Fig. 1b, and hence referred to as second order ladder term. Another possible pair occurs in the backscattering condition depicted in Fig. 2a, in which the field E_A travels in the same path as that in Fig. 1b, while the conjugate field E_B , starting from the transmitting antenna T, scatters first at point a and second at point b, eventually returning to the receiving antenna R. Since the fields E_A and E_B have the same path lengths, the correlation $\langle E_A E_B^* \rangle$ gives a finite value even for randomly distributed points a and b. This ray path of E_B is referred to as the time-reversal path of E_A . It is noted that the time reversal condition is satisfied only for the backscattering condition. As easily seen for the case of non-zero bistatic scattering angle, the fields E_A

Further author information: (Send correspondence to Satoru Kobayashi)
E-mail: satoru@radar-sci.jpl.nasa.gov, Telephone: 1 818-393-0824

and E_B have different path lengths, and random distributions of particles a and b will cause strong decorrelation, generally giving negligible contribution to the measured intensity. This is the reason we refer this additional contribution to intensity as backscattering enhancement. Regardless of the value of bi-static scattering angle, this conjugation scheme can be represented by the second order cross diagram depicted in Fig. 2b. In general, the ladder terms, such as shown in Fig. 1b, were proven to be equivalent to the multiple scattering terms calculated through the radiative transfer theory.³

For millimeter wave length radars, we can neglect the reflection from two-particle-correlation carried by turbulence.^{8,9} Thus in this paper, the incoherent scattering from each particle will be considered exclusively. For this incoherent scattering, backscattering enhancement was studied as a scalar theory in 5,6,10–13 and as a vector theory in 14–20. Numerical simulations for the vector theory were found in 21,22. Among these vector theories, the perturbation theories^{14,15,18–20} can be considered more appropriate for hydrometeors due to its small volume fraction of scatterers of order of 10^{-5} , comparing with the diffusion theories.^{16,17} Especially, two formalisms of Mishchenko^{19,20} and Mandt et al.¹⁴ are advantageous so as to have the explicit forms of scattering amplitude matrix in position-space representation. The former formalism includes all the contributions of ladder and cross terms, and seems to suit for numerical simulation, but not for analytical expression. The latter, on the other hand, includes at most the second order terms, but it can give an analytically simple form for a system of a finite layer thickness. Furthermore the second order theory can be considered to be sufficient for a dilute system such as hydrometeors as mentioned in 1,2.

In all the previous theoretical works, a plane wave is injected to randomly distributed particles, and the reflected wave is collected by a receiver at infinite range. On the other hand, in remote sensing, a spherical wave with a finite beam width, usually approximated as a Gaussian antenna pattern, is injected, and the reflected wave is received by an antenna at a finite range. For the single scattering, the plane wave theory can be applied to the spherical wave of a finite beam width with slight corrections concerning to range and gain, as will be also shown in this paper. While for multiple scattering, it is not appropriate to adopt the plane wave theory as it is, because a finite size footprint can be considered to give a smaller reflectivity than the plane wave theory predicts, especially when the footprint size is much smaller than the mean free path of an illuminated body. The mean free path in a layer of hydrometeors often reaches of the order of 1000 meters for millimeter-wavelength wave, while typical foot print sizes are of order of hundreds meters. In this study, a time-independent multiple scattering theory is formulated for a spherical wave along with a Gaussian antenna pattern, based on the plane wave theory of Mandt et al.¹⁴ Our analysis considers only a single layer of spherical water particles of a uniform diameter and a uniform number density.

2. FORMALISM

In this section, the formalism of Ishimaru, Tsang and Mandt^{10,14} is expanded to a spherical wave with a finite beam width represented by a Gaussian function. To deal with complication introduced by the finite beam width, further simplifications of integrals are performed for the second order ladder and cross terms.

We shall consider a single layer of hydrometeors of thickness d , constituted of spherical water particles of a uniform diameter D and a uniform density N_0 . To illustrate the backscattering enhancement, at first a bistatic radar is considered by assuming a small value of scattering angle θ_s , and later the formula for monostatic radar is derived by taking a limit of $\theta_s \rightarrow 0$. A 3-dB beam width θ_d and a range r_s are assumed to be $|\theta_d| \ll 1$ and $r_s \gg d$, respectively. When a radar of its center gain G_0 at a wavelength λ transmits a power of P_t with an initial polarization vector $\boldsymbol{\psi}_0$ in an incident direction \hat{k}_i , the first order scattering in a direction $\hat{k}_s (\approx -\hat{k}_i)$ can be represented by calculating the first order ladder term:

$$I_L^{(1)} = P_t G_0^2 \lambda^2 \theta_d^2 (2^7 \pi \ln 2 r_s^2)^{-1} N_0 \left\{ 2(\kappa''_{iz} + \kappa''_{sz}) \right\}^{-1} \sum_{\hat{\alpha}} \left| \langle \hat{\alpha} \left| F(-\hat{k}_i, \hat{k}_i) \right| \boldsymbol{\psi}_0 \right|^2 \left\{ 1 - \exp[-2(\kappa''_{iz} + \kappa''_{sz}) d] \right\} \quad (1)$$

in which the transmitting and receiving ranges have been assumed to be nearly equal. $F(\hat{k}_2, \hat{k}_1)$ denotes the scattering amplitude matrix from the directions \hat{k}_1 to \hat{k}_2 . The summation over unit vector $\hat{\alpha}$ is taken over a

complete set of polarizations such as the H and V directions. The absorption rates along the layer thickness are defined for the incident and scattered waves respectively:

$$\kappa''_{iz} = -\kappa_e/2\cos\theta_i \quad (2)$$

$$\kappa''_{sz} = \kappa_e/2\cos\theta_s \quad (3)$$

where θ_i and θ_s are the incident and scattered polar angles. The extinction rate κ_e is calculated through the Foldy-Twersky formula

$$\kappa_e = \text{Im} \left[4\pi N_0 k^{-1} F(\hat{k}_i, \hat{k}_i) \right] \quad (4)$$

in which k denotes the wavenumber. The footprint 3dB radius σ_r can be defined as

$$\sigma_r^2 = r_s^2 \theta_d^2 / 2^3 \ln 2 \quad (5)$$

Using the diagram of Fig. 1b, the second order ladder term for the finite beam width is calculated in the form of

$$\begin{aligned} I_L^{(2)} &= P_t G_0^2 \lambda^2 \theta_d^2 (2^7 \pi \ln 2 r_s^2)^{-1} N_0^2 \left\{ 2(\kappa''_{iz} + \kappa''_{sz}) \right\}^{-1} \\ &\int_0^\infty d\eta \int_0^{2\pi} d\varphi \int_0^d d\zeta \frac{\eta}{1+\eta^2} \exp[-\kappa_e \sqrt{1+\eta^2} \zeta] \exp[-\zeta^2 \eta^2 / 4\sigma_r^2] \\ &\sum_{\hat{\alpha}} \left\{ \left| \langle \hat{\alpha} | F(\hat{k}_s, \hat{r}) F(\hat{r}, \hat{k}_i) | \psi_0 \rangle \right|^2 \left[\exp\{-2\kappa''_{iz}\zeta\} - \exp\{2\kappa''_{sz}\zeta - 2(\kappa''_{iz} + \kappa''_{sz})d\} \right] \right. \\ &\left. + \left| \langle \hat{\alpha} | F(\hat{k}_s, -\hat{r}) F(-\hat{r}, \hat{k}_i) | \psi_0 \rangle \right|^2 \left[\exp\{-2\kappa''_{sz}\zeta\} - \exp\{2\kappa''_{iz}\zeta - 2(\kappa''_{iz} + \kappa''_{sz})d\} \right] \right\} \end{aligned} \quad (6)$$

In Eq. 6, the integrals over $\eta \equiv \tan\theta$ and φ concern to the polar coordinates of the directional variable \hat{r} that is defined inside inside the argument of the scattering amplitude matrix F . The other integral over $\zeta \equiv z_a - z_b$ is related to the relative coordinates of the direction of layer thickness.

The second order cross term for the finite beam width can be derived through the diagram of Fig. 2b in the form of

$$\begin{aligned} I_C^{(2)} &= P_t G_0^2 \lambda^2 \theta_d^2 (2^7 \pi \ln 2 r_s^2)^{-1} N_0^2 (\kappa''_{iz} + \kappa''_{sz})^{-1} \\ &\int_0^\infty d\eta \int_0^{2\pi} d\varphi \int_0^d d\zeta \frac{\eta}{1+\eta^2} \exp[-\{\kappa_e \sqrt{1+\eta^2} + \kappa''_{iz} + \kappa''_{sz}\} \zeta] \\ &\exp[-\zeta^2 \eta^2 / 4\sigma_r^2] \left\{ 1 - \exp[-2(\kappa''_{iz} + \kappa''_{sz})(d - \zeta)] \right\} \\ &\text{Re} \left[\left\{ \sum_{\hat{\alpha}} \langle \hat{\alpha} | F(\hat{k}_s, \hat{r}) F(\hat{r}, \hat{k}_i) | \psi_0 \rangle^* \langle \hat{\alpha} | F(\hat{k}_s, -\hat{r}) F(-\hat{r}, \hat{k}_i) | \psi_0 \rangle \right\} \exp[i(k_{dz} + t)\zeta] \right] \end{aligned} \quad (7)$$

in which the deviation vector \mathbf{k}_d from the backscattering direction and the new variable t have been introduced based on Ishimaru and Tsang¹⁰:

$$\mathbf{k}_d = k(\hat{k}_s + \hat{k}_i) \equiv k_{dx}\hat{x} + k_{dy}\hat{y} + k_{dz}\hat{z} \quad (8)$$

$$t \equiv k_{dx}\eta \cos\varphi + k_{dy}\eta \sin\varphi \quad (9)$$

3. RESULTS AND DISCUSSION

Multiple scatterings including backscattering enhancement can be considered to effectively increase radar reflectivity. When hydrometeors consist of spherical particles, the first order ladder term $I_L^{(1)}$ has only the copolarized component, i.e. $I_L^{(1)} = I_L^{(1)}(CO)$. Furthermore $I_L^{(1)}$ is almost constant in the vicinity of $\theta_s = 0$ ($\theta_s < 0.3$ degree), within which the backscattering enhancement occurs. For this reason, the intensity of a multiple scattering term will be normalized by $I_L^{(1)}$ to be converted to an effective reflectivity in the rest of paper. For instance, the second order ladder reflectivity in copolarized component denoted by L_2^{co} precisely means $I_L^{(2)}(CO)/I_L^{(1)}$.

The sums of only the second order terms $L_2^{co} + C_2^{co}$ in copolarization and $L_2^{cx} + C_2^{cx}$ in cross-polarization are plotted with the solid and dashed lines respectively in Fig. 3 as functions of the footprint radius normalized by the mean free path $l_0 = \kappa_e^{-1}$, (i.e. σ_r/l_0) to exclude the effect of the first order ladder term that is constant for σ_r/l_0 . Since the monostatic radar is our main concern, only the backscattering $\theta_s = 0$ will be considered hereinafter. Spherical water particles of a uniform diameter $D = 1$ mm with a particle number density $N_0 = 5 \times 10^3 \text{ m}^{-3}$ are used for calculation along with a frequency of 95 GHz, which gives the mean free path $l_0 = 77.2$ m. Figure 3 shows that the reflectivities rapidly decrease in the region $\sigma_r/l_0 < 1$, while these are almost constant in the region $\sigma_r/l_0 > 2$.

In Fig. 4, the terms $L_2^{co} + C_2^{co}$ (solid lines) and $L_2^{cx} + C_2^{cx}$ (dashed lines) are plotted as a function of optical thickness $\tau_d = d/l_0$ for several values of normalized footprint radius σ_r/l_0 . Here, only the frequency of 95 GHz and the particle diameter $D = 1$ mm are fixed. Since the mean free path l_0 is uniquely defined for an arbitrary particle density N_0 , the value of τ_d is changed by varying the physical layer thickness d . Using Fig. 4, we can determine reduction factor from the plane wave theory (i.e. $\sigma_r/l_0 = \infty$) for the particle diameter $D = 1$ mm, and given a footprint radius σ_r , a layer thickness d , and a particle number density N_0 . Figure 4 also indicates that the plane wave theory can be applied to a smaller value of σ_r/l_0 , as the optical thickness decreases. For example, at a large optical thickness $\tau_d = 4.0$, the values of $L_2^{co} + C_2^{co}$ (Solid lines) are -1.89 dB and -2.39 dB for $\sigma_r/l_0 = \infty$ and $\sigma_r/l_0 = 1$ respectively. These values reduce to -11.49 dB and -11.58 dB respectively at a small optical thickness $\tau_d = 0.05$. Hence the difference in $L_2^{co} + C_2^{co}$ between $\sigma_r/l_0 = \infty$ and $\sigma_r/l_0 = 1$ is given by 0.50 dB at $\tau_d = 4$, which reduces to 0.09 dB at $\tau_d = 0.05$. In short, the curve of $\sigma_r/l_0 = \infty$ approximately coincides with the curve of $\sigma_r/l_0 = 1$ at $\tau_d = 0.05$. Thus the plane wave theory can be applied for the footprint radius $\sigma_r/l_0 = 1$ at a small $\tau_d = 0.05$.

4. CONCLUSION

In this paper, a vector theory, involving up to the second order scattering, has been studied for a finite footprint radius along with a moderate single particle albedos ($\lesssim 0.5$) and optical thicknesses ($\tau_d \leq 4$), although the approximation is highly valid for $\tau_d \lesssim 2$. As the optical thickness of the hydrometeor layer increases, the differences from the conventional plane wave theory become significant, and essentially the reflectivity of multiple scattering depends on the ratio of radar footprint radius to mean free path as shown in Fig. 4. For a single layer of hydrometeors with a uniform diameter D , we can theoretically estimate the effect of multiple scatterings for a finite footprint radius by making a corresponding figure to Fig. 4 for the given diameter D . Especially for the Rayleigh regime, similarities of curve shapes in Fig. 4 hold, and the difference for D appears only in magnitude proportional to D^6 , which makes calculation of Fig. 4 simpler. Although the dependence of the particle density N_0 does not appear explicitly in Fig. 4, it is implicitly included in the mean free path l_0 . Thus we still need rough information on N_0 and D , which may be obtained, for instance, through cooperation of a Ku-band radar that has very little effect of multiple scattering. Once N_0 and D are roughly given, the measured reflectivity in cross-polarization is used to confirm the degree of multiple scattering, and the information from Fig. 4 redrawn for the given D , in turn, gives correction for the multiple scattering in the copolarized reflectivity.

An issue to be considered in this paper is that all the formalism have been done under the restriction of a single layer of spherical hydrometeors with a uniform number density N_0 and a uniform diameter D . We can extend the formalism of this paper to a more general shaped hydrometeors by adding integrals relating ensemble averages of particle orientations as well as drop size distribution. Preliminary results expanded to a single layer of hydrometeors with the Marshall-Palmer distribution are shown in Appendix A.

The theory in this paper has been derived for continuous wave as a time-independent theory. However we may extend it to a time-dependent theory to apply to a short pulsed radar. For a single layer of hydrometeors composed of spherical particles, a convenient formula of the time-dependent radiative transfer theory was derived as a second order analytical solution by Ito et al.¹ Since the cross term behaves in a similar manner to the ladder term for the backscattering within the second order theory, the backscattering enhancement can be involved in the solution of Ito et al.¹ by formerly multiplying the factor of 2 to its second order term. It is further noted that their solution was derived for the plane wave. We therefore need to multiply the above-mentioned second order term by the reduction factor arising from the finite footprint radius, which is obtained from Fig. 4 or its counterpart extended to a more general drop size distribution of particles.

APPENDIX A. MULTIPLE SCATTERING WITH MARSHALL-PALMER DISTRIBUTION

As a preliminary result, increments in reflectivity to single scattering intensity are plotted as functions of rain rate (mm/hr) for the Marshall-Palmer distribution along with a frequency of 95 GHz in Fig. 5a, in which the infinite footprint radius and a layer thickness of 100 m are assumed. Solid and dashed lines denote the total increments in copolarized and cross-polarized reflectivities, respectively. The upper curves in each polarization include backscattering enhancement, while the lower curves not. Figure 5a indicates that the increment in copolarized reflectivity reaches over 1 dB for stratiform rains of 10 mm/hr.

In Fig. 5b, using the finite beam theory, the second order reflectivities in both polarizations are plotted as functions of the normalized footprint radius σ_r/l_0 for the rain rate of 10 mm/hr corresponding to the mean free path $l_0 = 528$ m. The same layer thickness as Fig. 5(a) is used. Since the values at $\sigma_r/l_0 = 4$ can be regarded approximately as the values at $\sigma_r/l_0 = \infty$, we can retrieve the reflectivities ($L_2^{cx} + C_2^{cx}$, $1 + L_2^{co} + C_2^{co}$) in Fig. 5a at rain rate 10 mm/hr, directly from the value of $L_2^{cx} + C_2^{cx}$ in Fig. 5b for cross-polarization, while by calculating $1 + L_2^{co} + C_2^{co}$ from the value of $L_2^{co} + C_2^{co}$ in Fig. 5b for copolarization.

REFERENCES

1. Ito, S., T. Oguchi, H. Kumagai, and R. Meneghini, "Depolarization of radar signals due to multiple scattering in rain", *IEEE Trans. Geosci. and Remote sensing*, **33**, pp. 1057-1062, 1995.
2. Iguchi, T., R. Meneghini, and H. Kumagai, "Radar depolarization signatures of rains in cumulus clouds measured with dual-frequency air-borne radar", *Proc. IGARSS'92 Symp.*, pp. 1728-1730, 1992.
3. Tsang, L., and J. A. Kong, *Scattering of electromagnetic waves: Advanced topics*, John Wiley & Sons, Inc., New York, 2001.
4. de Wolf, D. A., "Electromagnetic reflection from an extended turbulent medium: Cumulative forward scatter single-backscatter approximation", *IEEE Trans. Antenna and Propag.*, **Ap-19**, pp. 254-262, 1971.
5. Golubentsev, A. A., "Suppression of interference effects in multiple scattering of light", *Soviet Phys. JETP*, **59**, pp. 26-32, 1984.
6. Tsang, L. and A. Ishimaru, "Theory of backscattering enhancement of random discrete isotropic scatterers based on the summation of all ladder and cyclical terms", *J. Opt. Soc. Am. A.*, **2**, pp. 1331-1338, 1985.
7. Kravtsov, Yu., and A. I. Saichev, "Effects of double passage of waves in randomly inhomogeneous media", *Sov. Phys. Usp.*, **25**, pp. 494-508, 1982.
8. de Wolf, D. A., W. J. Russchenberg, and L. P. Ligthart, "Radar reflection from clouds: Gigahertz backscatter cross sections and Doppler spectra", *IEEE Trans. Antenna Propag.*, **48**, pp. 254-259, 2000.
9. Kobayashi, S., "A unified formalism of incoherent, quasi-coherent and coherent correlation signals on pulse-pair Doppler operation for cloud -profiling radar for a space mission", *J. Atmos. Ocean. Tech.*, **19**, pp. 443-456, 2002.
10. Ishimaru, A., and L. Tsang, "Backscattering enhancement of random discrete scatterers of moderate sizes", *J. Opt. Soc. Am. A.*, **5**, pp. 228-236, 1989.
11. Akkermans, E., P. E. Wolf, and R. Maynard, "Coherent backscattering of light by disordered media: Analysis of the peak line shape", *Phys. Rev. Lett.*, **56**, pp. 1471-1474, 1988.

12. Barbanenkov, Yu, and V.D. Ozrin, “Coherent enhancement of back-scattered radiation in a randomly inhomogeneous medium: the diffusion approximation”, *Soviet Phys. JETP*, **67**, pp. 1117-1121, 1988.
13. Tsang, L. and A. Ishimaru, “Backscattering enhancement of random discrete scatterers”, *J. Opt. Soc. Am. A.*, **1**, pp. 836-839, 1984.
14. Mandt, C. E., L. Tsang, and A. Ishimaru, “Copolarized and depolarized backscattering enhancement of random discrete scatterers of large size based on second-order ladder and cyclical theory”, *J. Opt. Soc. Am. A.*, **7**, pp. 585-592, 1989.
15. Mandt, C. E., and L. Tsang, “Backscattering enhancement from a random distribution of large discrete spherical scatterers with a size distribution”, *J. Opt. Soc. Am. A.*, **9**, pp. 2246-2251, 1992.
16. Akkermans, E., P. E. Wolf, R. Maynard, and G. Maret, “Theoretical study of the coherent backscattering of light by disordered media”, *Journal de Physique*, **49**, pp. 77-98, 1988.
17. Stephen, M. J., and G. Cwilich, “Rayleigh scattering and weak localization: Effect of polarization”, *Phys. Rev. B.*, **34**, pp. 7564-7572, 1986.
18. V.L. Kuzmin, V.P. Romanov and V.L. Kuzmin, “Depolarization of coherent backscattering”, *Optics and Spectroscopy*, **72**, pp. 125-130, 1992
19. Mishchenko, M.I., “Polarization effects in weak localization of light: Calculation of the copolarized and depolarized backscattering enhancement factors”, *Phys. Rev. B*, **44**, pp. 12597-12600, 1991.
20. Mishchenko, M.I., “Enhanced backscattering of polarized light from discrete random media: calculations in exactly the backscattering direction”, *J. Opt. Soc. Am. A.*, **9**, pp. 978-982, 1992.
21. Oguchi, T., and T. Ihara, “Numerical simulation of backscattering enhancement from modeled rain drops in millimeter wave length”, *URSI F Japanese committee Report*, **Dec.**, pp. 1-5, 2003.
22. van Albada, M. P., and Ad. Lagendijk, “Vector character of light in weak localization: Spatial anisotropy in coherent backscattering from a random medium”, *Phys. Rev. B.*, **36**, pp. 2353- 2356, 1987.

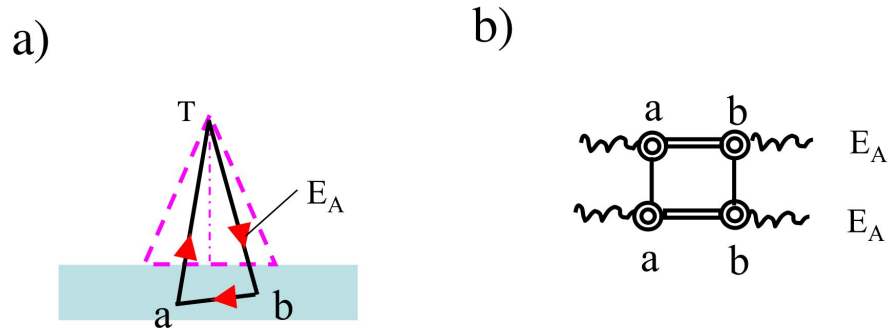


Figure 1. Second order ladder term. An incident field E_A emits from the antenna T, and scatters at points 'b' and 'a' successively in the random media, returning to the antenna T. (a): Geometry. (b): Diagram.

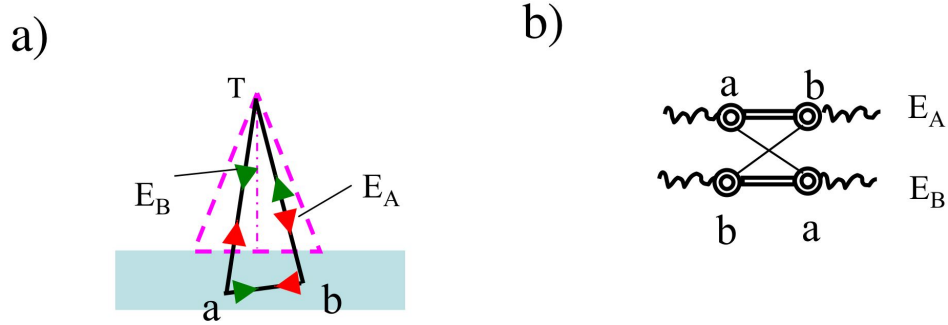


Figure 2. Second order cross term. An incident field E_A takes the same path as in Fig. 1b, while the conjugate field E_B emits from the antenna T, and scatter at points 'a' and at 'b' successively (i.e. time-reversal path of E_A), returning to the antenna T. (a): Geometry. (b): Diagram.

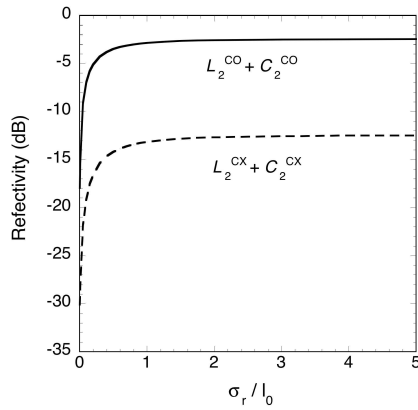


Figure 3. The reflectivity $L_2^{co} + C_2^{co}$ in copolarization (solid line) and the reflectivity $L_2^{cx} + C_2^{cx}$ in cross-polarization (dashed line) as functions of the normalized footprint radius σ_r / l_0 for the backscattering $\theta_s = 0$. Spherical water particle of diameter $D = 1$ mm and particle number density $N_0 = 5 \times 10^3 \text{ m}^{-3}$ are used, which give the mean free path $l_0 = 77.2$ m

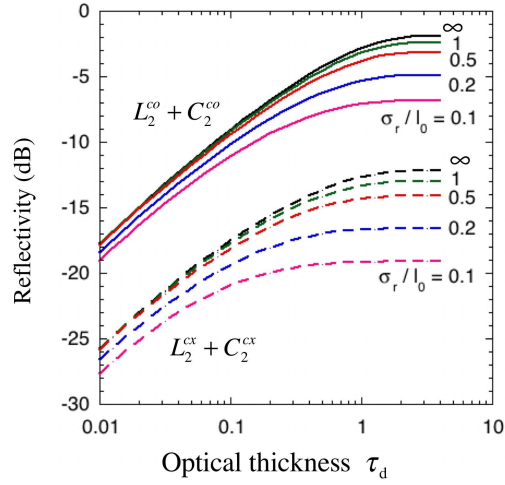


Figure 4. The reflectivity $L_2^{co} + C_2^{co}$ in copolarization (solid lines) and the reflectivity $L_2^{cx} + C_2^{cx}$ in cross-polarization (dashed lines) as functions of the optical thickness τ_d for the backscattering $\theta_s = 0$. Hydrometeor diameter is set at $D = 1$ mm. Particle number density N_0 is arbitrary. The parameters of footprint radius σ_r/l_0 are set at ∞ , 1, 0.5, 0.2 and 0.1 from top to down. The differences of finite footprint radius ($\sigma_r/l_0 = 1 - 0.1$) from the plane wave theory ($\sigma_r/l_0 = \infty$) reduce, as τ_d decreases.

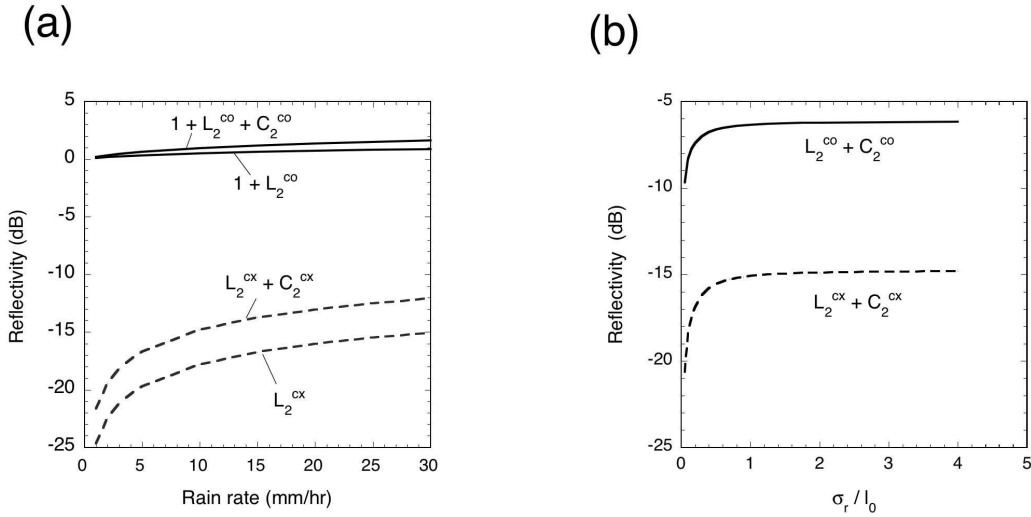


Figure 5. (a) Increments in total reflectivities as functions of rain rate (mm/hr) for Marshall-Palmer distribution. Frequency 95 GHz and a layer thickness of 100 m are assumed. Solid and dashed lines correspond to copolarization and cross-polarization, respectively. (b) Second order reflectivities as functions of the normalized footprint radius σ_r/l_0 for a rain rate of 10 mm/hr. The same layer thickness as (a) is used. The solid and dashed lines correspond to copolarization and cross-polarization, respectively.